Materials Today Bio 17 (2022) 100460

Contents lists available at ScienceDirect

Materials Today Bio

journal homepage: www.journals.elsevier.com/materials-today-bio

A microfluidic model of human vascularized breast cancer metastasis to bone for the study of neutrophil-cancer cell interactions

Martina Crippa [a,b,c], Giuseppe Talò [d], Anaïs Lamouline [a,b,c], Sara Bolis [e], Chiara Arrigoni [a,b,f], Simone Bersini [a,b,f,*,1], Matteo Moretti [a,b,d,f,**,1]

[a] Regenerative Medicine Technologies Lab, Ente Ospedaliero Cantonale, 6500, Bellinzona, Switzerland
[b] Service of Orthopaedics and Traumatology, Department of Surgery, Ente Ospedaliero Cantonale, 6900, Lugano, Switzerland
[c] Department of Electronics, Information and Bioengineering, Politecnico di Milano, Milano, Italy
[d] Cell and Tissue Engineering Lab, IRCCS Istituto Ortopedico Galeazzi, Milano, Italy
[e] Laboratory for Cardiovascular Theranostics, Istituto Cardiocentro Ticino, Ente Ospedaliero Cantonale, 6500, Bellinzona, Switzerland
[f] Faculty of Biomedical Sciences, Università della Svizzera Italiana, 6900, Lugano, Switzerland

ARTICLE INFO

Keywords:
Biofabrication
Microfluidics
Bone metastasis
Neutrophil
Microvascular network

ABSTRACT

The organ-specific metastatization of breast cancer to bone is driven by specific interactions between the host microenvironment and cancer cells (CCs). However, it is still unclear the role that circulating immune cells, including neutrophils, play during bone colonization (i.e. pro-tumoral vs. anti-tumoral). Here, we aimed at analyzing the migratory behavior of neutrophils when exposed to breast CCs colonizing the bone and their contribution to the growth of breast cancer micrometastases. Based on our previous bone metastasis models, we designed a microfluidic system that allows to independently introduce human vascularized breast cancer metastatic seeds within a bone-mimicking microenvironment containing osteo-differentiated mesenchymal stromal cells and endothelial cells (ECs). ECs self-assembled into microvascular networks and connected the bone-mimicking microenvironment with the metastatic seed. Compared to controls without CCs, metastatic seeds compromised the architecture of microvascular networks resulting in a lower number of junctions (5.7 ± 1.2 vs. 18.8 ± 4.5, $p = 0.025$) and shorter network length (10.5 ± 1.0 vs. 13.4 ± 0.8 [mm], $p = 0.042$). Further, vascular permeability was significantly higher with CCs ($2.60 \times 10^{-8} \pm 3.59 \times 10^{-8}$ vs. $0.53 \times 10^{-8} \pm 0.44 \times 10^{-8}$ [cm/s], $p = 0.05$). Following metastatic seed maturation, neutrophils were injected into microvascular networks resulting in a higher extravasation rate when CCs were present (27.9 ± 13.7 vs. 14.7 ± 12.4 [%], $p = 0.01$). Strikingly, the percentage of dying CCs increased in presence of neutrophils, as confirmed by confocal imaging and flow cytometry on isolated cells from the metastatic seeds. The biofabricated metastatic niche represents a powerful tool to analyze the mechanisms of interaction between circulating immune cells and organ-specific micrometastases and to test novel drug combinations targeting the metastatic microenvironment.

1. Introduction

The formation of metastases in distant sites still represents the principal cause of cancer related death [1]. In this context, specific tissues including bone are particularly prone to host metastases from a wide set of primary tumors such as breast, prostate, lung and kidney tumors [2]. Although the organ-specific metastatization of these tumors to bone is well documented, a complete understanding of the mutual role of host microenvironment and tumor phenotype in bone metastasis formation is still missing [3]. The bone microenvironment provides an immune privileged niche, constituted by a wide variety of immune cells that are actively involved in the metastatic process [4]. Hence, identifying the interactions between immune cells and disseminating cancer cells (CCs) would represent a critical aspect to design more effective therapies targeting bone metastases [5].

Unfortunately, efforts to clarify immune-CC interactions highlighted how different immune cell types (e.g. neutrophils, macrophages, monocytes) can both inhibit and promote the metastatic disease in different

* Corresponding author. Regenerative Medicine Technologies Lab, Ente Ospedaliero Cantonale, 6500, Bellinzona, Switzerland.
** Corresponding author. Regenerative Medicine Technologies Lab, Ente Ospedaliero Cantonale, 6500, Bellinzona, Switzerland.
E-mail addresses: simone.bersini@eoc.ch (S. Bersini), matteo.moretti@eoc.ch (M. Moretti).
[1] Equally contributing authors.

https://doi.org/10.1016/j.mtbio.2022.100460
Received 22 June 2022; Received in revised form 28 September 2022; Accepted 8 October 2022
Available online 10 October 2022

tissues including bone [6]. Indeed, CCs can alter the physiological immune cell behavior inducing a specific tumor-associated phenotype. In this context, Tumor Associated Macrophages (TAMs) were one of the first immune populations to be extensively studied for their interactions with primary and metastatic tumors [7]. In particular, macrophages demonstrated to have functional plasticity being able to change their polarization from an anti-tumor, pro-inflammatory phenotype (i.e. M1) to a pro-tumor, immune suppressive cell type (i.e. M2) [8,9].

Based on these observations, a similar paradigm was recently used to characterize the polarization of Tumor Associated Neutrophils (TANs) [10,11], whereby N1 neutrophils show an anti-tumor and N2 neutrophils a pro-tumor phenotype [7,12]. Neutrophils represent the largest leukocyte population in blood and constitute the greatest portion of tumor infiltrated inflammatory cells in multiple cancer models. Further, neutrophils play an important role in the tumor microenvironment since they produce cytokines and chemokines responsible for the recruitment and activation of other immune cell types [7,10,13]. Although neutrophils are now considered a relevant cell type contributing to the establishment of metastases, their role is still controversial. For instance, transforming growth factor (TGF)-β secreted by the tumor microenvironment was reported to drive TANs towards an N2 phenotype, suggesting how its blockade through soluble receptors or antibodies could represent a promising anti-tumor treatment [12]. In the context of breast cancer osteolytic bone metastases, TGF-β is also one of the main factors released by the bone matrix degradation that could shift the balance towards pro-tumor N2 neutrophils [4]. However, it should also be considered that other studies pointed out how tumor-entrained neutrophils can impair the metastatic process [12,14] also through the release of cytotoxic molecules [12]. Summarizing, the role of neutrophils in tumor biology has not yet been fully clarified, also suggesting potential differences in neutrophil behavior between primary vs. secondary tumors as well as early stage vs. late stage metastases [15]. Another key aspect regarding neutrophil interaction with both primary and metastatic tumors is their recruitment through the microvasculature. Indeed, both endothelial cells (ECs) and supporting fibroblasts secrete chemo-attractive cytokines (e.g. interleukin (IL)-1β, IL-17, tumor necrosis factor (TNF)-α) [11]. In addition, ECs express integrins and selectins (e.g. P-selectin, E-selectin) that promote neutrophil adhesion and extravasation. In this scenario, it is still not clear to which extent molecular changes occurring to tumor associated ECs as well as alterations to the architecture of the microvascular system of tumors can affect neutrophil behavior and their active migration. This concept is especially true for highly vascularized tissues including bone.

Since the identification of TANs, the interplay between CCs and neutrophils was mainly investigated through the analysis of patient samples [16] and *in vivo* models [17,18]. These approaches led for instance to the development of innovative strategies to impair neutrophil migration and recruitment to the tumor microenvironment [19]. Recently, innovative *in vitro* 3D vascularized microphysiological systems were designed to analyze the role of neutrophils during CC extravasation and metastasis formation [20,21]. Other microfluidic platforms were also specifically designed to study the migration of neutrophils themselves [22]. Although these models significantly contributed to increasing our knowledge of key mechanisms of neutrophil migration and interaction with CCs, they did not take into account the importance of organ-specificity during the formation of metastases or they simply included external factors (e.g. lipopolysaccharides) which poorly mimic the inflammatory tumor microenvironment and skew neutrophil polarization. Moreover, these models did not allow to easily recover CCs following their interaction with neutrophils and then characterize their phenotype through quantitative analyses.

Based on our previously developed microscale and mesoscale bone-mimicking metastasis assays [23,24], here we present a model of perfusable microvascular network that connects a healthy bone-mimicking microenvironment with an already established breast cancer metastasis to bone (BMtB) where circulating neutrophils can be injected and live tracked to follow their interaction with CCs. A key aspect of the described microfluidic device is the possibility to independently biofabricate the bone microenvironment and multiple metastatic seeds, which then integrate with the surrounding microvasculature. This BMtB-on-a-chip allowed us to analyze how the metastatic microenvironment influences neutrophil migration and the ensuing interactions with CCs through a combination of single-cell imaging and quantitative flow cytometry analyses on retrieved live cells.

2. Materials and methods

2.1. Design of the microfluidic device

The microfluidic device was designed with computer-aided design (CAD) (Solid Edge, Siemens) (Fig. 1A) and the mold was printed with a photopolymerizable resin using a high-resolution 3D printer (Fig. 1B). To obtain the devices, poly-dimethyl-siloxane (PDMS, SYLGARD®184, Dow Chemical Company) was poured on the mold and cured in an oven at 65 °C for 2 h. Once polymerized, the PDMS was removed from the mold, allowing to obtain 4 mm inlets/outlets for the media channels and 1 mm inlets/outlets for the hydrogel channels. The PDMS was attached to glass microscope slides or coverslips through plasma bonding. The obtained microfluidic chip consisted of three independent circular hydrogel regions (1 mm diameter) physically separated from each other and surrounded by two hydrogel channels (300 μm high, 1 mm wide), each one flanked by two lateral media channels (300 μm high, 1 mm wide). Each circular hydrogel region was separated from the hydrogel channels by PDMS lips (150 μm high), which allowed the confinement of the hydrogel matrix. Similar lips were used to separate the hydrogel channels from the media channels. An internal wall separates the two hydrogel channels, hence forcing the flow through the circular hydrogel regions.

2.2. Cell culture and seeding procedure of the microfluidic device

Following microfabrication and sterilization of the microfluidic chip, we generated the BMtB including two different microenvironments. Firstly, we seeded inside the three circular regions the BMtB microenvironment, composed of green fluorescent protein (GFP)-transfected human umbilical vein endothelial cells (HUVECs, Angioproteomie; final density 6×10^6 cells/ml), bone mesenchymal stem cells (BMSCs, a pool isolated from knee biopsies of 4 donors; final density 0.15×10^6 cells/ml), fibroblasts (Lonza; final density 0.15×10^6 cells/ml), and red fluorescent protein (RFP)-transfected MDA-MB-231 (Angioproteomie; final density 0.75×10^6 cells/ml). Outside the circular regions, in the two hydrogel channels we generated a "vascularized bone-mimicking microenvironment", consisting of a suspension of GFP-transfected ECs (final density 4×10^6 cells/ml), fibroblasts (final density 0.1×10^6 cells/ml), BMSCs and osteo-differentiated BMSCs (O-BMSCs) (both at the same final density 0.1×10^6 cells/ml). The presence of fibroblasts in the model is fundamental to promote the formation of a branched and interconnected microvascular network. The O-BMSCs were cultured before seeding in the devices for 14 days with osteogenic medium (Dulbecco's modified Eagle medium (DMEM; 4.5 g/L glucose, Life Technologies), 10% fetal bovine serum (FBS), 2 mM L-glutamine, 1 mM sodium pyruvate, 10 mM HEPES, 1 U/ml penicillin and 1 μg/ml streptomycin supplemented with 0.01 μM dexamethasone, 10 mM β-glycerophosphate, 10 nM cholecalciferol, 150 μM L-ascorbic acid-2-phosphate (Sigma Aldrich)) [25]. The OsteoImage Mineralization assay (Lonza) was used to assess the presence of hydroxyapatite deposits. Both the cell mixtures were resuspended in a solution of endothelial growth medium (EGM)-2MV (Lonza) containing 4 IU/ml thrombin (Baxter) to promote fibrinogen polymerization and form a stable fibrin matrix. Then, the suspension containing cells and thrombin was 1:1 mixed with a 10 mg/ml fibrinogen solution and injected in the three circular regions from above (BMtB microenvironment) and within the two hydrogel channels from their inlets (vascularized bone-mimicking microenvironment). Overall, 5

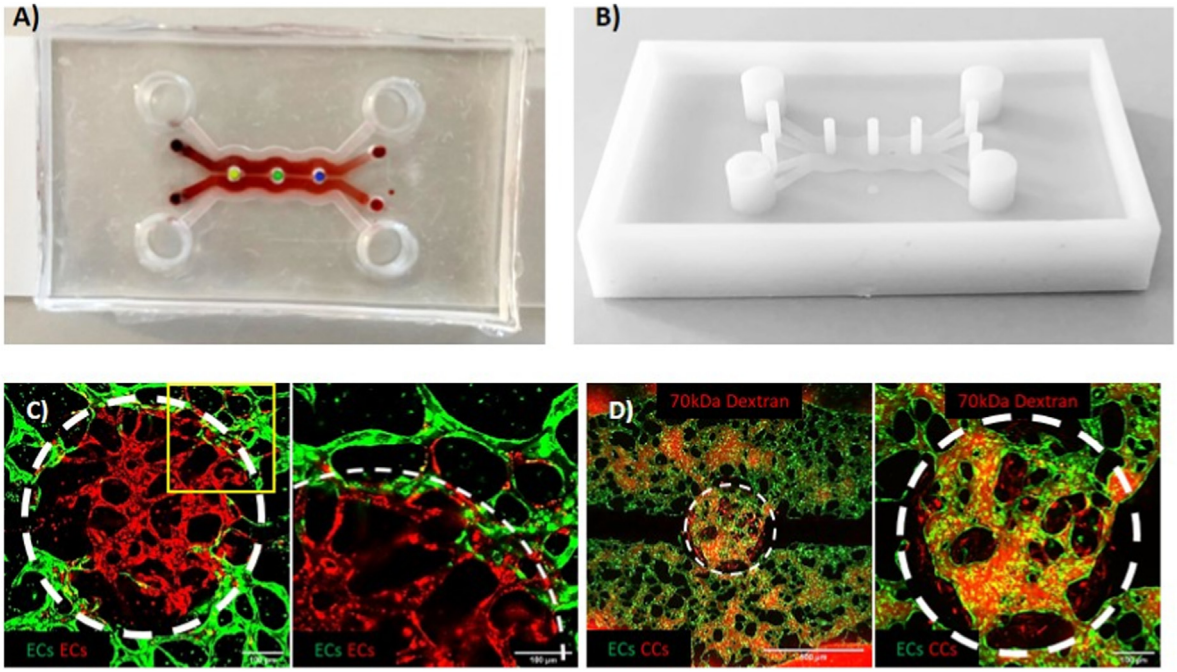

Fig. 1. Microfluidic design of the BMtB model. Image of the device bonded with dyed hydrogels, red for the gel channels and yellow, green and blue for each circular region. The image was obtained superimposing the separate image of the red gel within the channels with the image of the gels within the circular regions that were artificially colored to better show the different compartments of the device (A). Image of the 3D printed mold (B). Representative confocal images showing the network connection between GFP ECs within the hydrogel channel and RFP ECs within one of the circular regions at day 4 of culture (C, 10X (left), 20X (right)). A yellow square on left image points to the area magnified in the right image. Representative confocal images capturing the flow of 70 kDa TRITC Dextran within microvascular networks connecting the hydrogel channels with one of the metastatic regions (D, 4X (left), 10X (right)). The circular region borders are highlighted with a white dotted circumference. (For interpretation of the references to colour in this figure legend, the reader is referred to the Web version of this article.)

mg/ml fibrin hydrogels were formed upon polymerization in the circular regions and within the channels. After 20 min gelation in a humified chamber, the media channels were filled with EGM-2MV. To nourish the three "BMtB microenvironments" and to promote vessel development, a droplet of 100 μl medium enriched with Vascular Endothelial Growth Factor (VEGF 50 ng/ml; Thermofisher) was poured on top of them. The medium was replenished every day until the fourth day of culture when mature and perfusable vascular networks were formed. Due to the configuration of the chip, in which the circular regions are the only way to connect the two hydrogel channels containing microvascular networks, the perfused medium and neutrophils were forced to pass across the three BMtB microenvironments.

Neutrophils were isolated from commercially available human buffy coats the day of the seeding into microfluidic devices following already established protocols [20]. A preliminary centrifugation step with Ficoll (Sigma) gradient allowed to separate blood components according to their density, then neutrophils were incubated for 1 h in 3% dextran T500 (Sigma) and purified from red blood cells with Red Blood Cell Lysis Solution (Miltenyi). Isolated neutrophils were suspended in EGM-2MV at a concentration corresponding to the average physiological density (3.5×10^6 cells/ml) for the preliminary 2D tests and at the highest physiological concentration (8×10^6 cells/ml) for the injection in the microfluidic devices. We used the highest neutrophil concentration to overcome the possible dispersion of these cells within the microvascular network.

2.3. Analysis of the effect of neutrophils on CCs in co-culture

As a preliminary test of the effect of neutrophils on CCs, 2D co-culture experiments were set in which 96-multiwell plates with monolayers of CCs (density 0.015×10^6 cells/ml) were prepared two days before the isolation of blood components. Then, the neutrophil suspension (density 3.5×10^6 cells/ml) was incubated with CCs and the effects of the co-culture were quantified at 24 h. We also preliminary evaluated CC viability within a 3D environment by embedding CCs alone or co-cultured with the BMtB cells in fibrin gel (final density 0.75×10^6 cells/ml), with or without neutrophils (density 3.5×10^6 cells/ml), evaluating them at the same time point.

At the end of the experiment, the medium was removed, the cells were washed with PBS and each well was acquired (10× magnification) with an epifluorescence microscope (Nikon). The effect of neutrophils on the CC monolayer was quantified by analyzing the area covered by CCs at each time point (through the function *Area fraction* of the *Analyze function* of Fiji software). In the case of CCs embedded in fibrin gel, CC viability was obtained by quantifying the number of DRAQ7 positive cells (far-red fluorescent dye, Dead Cell Exclusion; Abcam). In detail, the Fiji plugin *Colocalization* was used to selectively evaluate CC mortality, excluding from the count the signals of dead neutrophils. To assess the CC mortality both the RFP (CCs) and the DAPI (Neutrophils) channels were colocalized with the far-red channel (Draq7) of the same region of interest (ROI). This passage allowed to obtain the representation of dead CCs and neutrophils, separately.

For the analysis of cellular reactive oxygen species (ROS) on CCs, a red fluorescence detection assay kit (ab186027, Abcam) was used. To avoid overlapping between the RFP signal of MDA-MB-231 and of the red fluorescence ROS kit, non-fluorescent MDA-MB-231 were embedded in fibrin gels, as already described in previous sections. Following the manufacturer protocol, cells were treated with the ROS detection working solution for 30 min before the addition of neutrophils. The images were acquired live after 24 h incubation using an epifluorescence microscope (Nikon). The intensity of the ROS signal was analyzed by evaluating the mean gray value using Fiji.

2.4. Analysis of microvascular network features

The microvascular network features were analyzed obtaining a binary

mask of the network through the Fiji plugin *Trainable Weka Segmentation*, which through machine learning algorithms generates pixel-based segmentation from the selection of a set of image features. Then, the networks were analyzed with the Fiji functions *Skeletonize* and *Analyze Skeleton* in terms of number of branches, number of junctions, average branch length and area occupied by the network.

2.5. Analysis of microvessel permeability

The perfusability of the microvascular network was tested by removing the medium from the reservoirs of the device and injecting in one medium inlet 10 μl 70 kDa TRITC Dextran (2.5 mg/ml, Chondrex). The permeability of the networks was calculated by analyzing the stack images of Dextran injection obtained using a confocal microscope (Nikon). The images were acquired live for 10 min with a z-step of 10 μm and a time-step of 30 s at 10× magnification focusing on the circular regions of the microfluidic devices. For each image, 3 smaller ROIs (100 μm × 100 μm) were considered and through an already developed Fiji macro [26] it was possible to obtain the variation of the fluorescence intensity (ΔI) between the network and the hydrogel, comparing the first and the last time points. These values were then used to obtain the permeability P [cm/s], which represents the resistance per surface area (SA) offered by the endothelial wall of the network against the solute flux (Js [mols^{-1}]) driven by the transendothelial difference of concentration (Δc). The permeability P [cm/s] of the networks was obtained by solving the following equation, which is derived by the Fick law ($Js = P*SA*(C_{network}-C_{gel})$) equaled to the equation of the mass conservation of the hydrogel ($Js = V_m*(dC_{gel}/dt)$). The difference of concentration (Δc) was considered equal to the variation of fluorescence intensity (ΔI) [26]:

$$\boldsymbol{P}=\frac{\boldsymbol{V_m}}{\boldsymbol{SA}\,\boldsymbol{\Delta I}}\,\frac{\boldsymbol{\Delta I_m}}{\boldsymbol{t}}$$

where SA and V_m are the surface area and the matrix volume, respectively, ΔI is the fluorescence intensity difference between the network and the hydrogel at the first time point, while ΔI_m represents the increased fluorescence intensity in the hydrogel during the time interval t[26].

2.6. Evaluation of cell mortality and neutrophil extravasation on chip

To quantify the extravasation of neutrophils and CC mortality, stack images (10X, 10 μm step) of the circular regions of the devices were real-time acquired using a confocal microscope (Nikon). For the quantification of CC death, the same procedure previously described for the quantification of CC death in the hydrogel droplets was used. Briefly, this procedure consists of the initial evaluation of the colocalized signals (*Colocalization* plugin) between the different fluorescence channels of a Z-stack, followed by the subtraction of overlapped signals. In particular, the far-red channel (Draq7, dead cells) was colocalized with the DAPI (neutrophils), RFP (CCs) and GFP (ECs) channels. Then, the colocalized signals between Draq7-neutrophils and Draq7-ECs were both subtracted to the colocalized Draq7-CC signal. This way, the CC death signal was cleaned by potential artifacts due to the tridimensionality of the structure. The resulting images were then numerically quantified in terms of area or number of spots through *Analyze particles* command. For what concerns neutrophil extravasation, firstly the colocalization between DAPI (neutrophils) and GFP (ECs) was measured, to obtain the number of neutrophils within the microvascular network. This value was then subtracted to the original neutrophil channel to obtain the number of extravasated neutrophils. The quantitative analysis was then performed using the *Analyze particles* command.

2.7. Isolation of cells from the BMtB regions

24 h after neutrophil injection within microfluidic devices, a biopsy puncher with a diameter of 3 mm was used to collect the hydrogel portions in the circular regions. Three circular regions of two devices for each condition were collected and pooled together. The fibrin gel was degraded using Nattokinase (1 mg/ml in PBS, JBSL) at 37 °C for 1 h [24], pipetting every 10 min to promote the detachment of the hydrogel from the PDMS and its degradation. After hydrogel degradation, the cells were pelleted, washed with PBS and processed for further analyses.

2.8. Flow cytometry analysis

The Flow cytometry tests were performed with the flow cytometer CytoFLEX S (Beckman Coulter) and the results were analyzed with Kaluza Analysis Software (Beckman Coulter). Regarding the viability test of CCs isolated from the circular regions of the microfluidic devices, all the cell types of the breast metastasis microenvironment were previously analyzed (alone and in combination) to properly set the thresholds that were then applied to the cells collected from the devices. This passage was useful in particular to distinguish transfected cells (RFP-MDA and GFP-HUVECs) and to exclude a priori any possible signal overlap with Draq7, that was used to determine cell death.

For the analysis of neutrophil marker expression, 3 wells of a 48-well plate for each condition (neutrophils alone and in coculture with CCs for 24 h) were pooled, centrifuged and the pellet was resuspended in 350 μl FACS Buffer (PBS + 0.1% Human Serum Albumin + 500 ng/μl IgG, Sigma). 100 μl of these suspensions were added to previously prepared 96-well plates containing a mix of antibodies and isotypes. The isotypes used were the following: IgG1-FITC (100 ng, Miltenyi), IgG1-APC (100 ng, Miltenyi), and IgG1-PC7 (100 ng, BD-Pharmingen). The antibodies used were: CD120α-APC and CD120β-APC (100 ng, Miltenyi and BioLegend), CD95-FITC (100 ng, BioLegend), CD15-FITC (100 ng, BD-Pharmingen) and CD274-PC7 (100 ng, eBioscience). Antibody dilutions were set accordingly to the manufacturer's recommendations. The cell suspensions were incubated in dark for 20 min at room temperature (RT), then 80 μl PBS were added and the acquisition was performed measuring the median fluorescence intensity. The values of the isotypes were then subtracted to the obtained values and the results of the treated condition (coculture with CCs) were normalized to the controls (neutrophils alone).

2.9. Immunofluorescence and live imaging

Samples were fixed with 2% paraformaldehyde (PFA) for 10 min, treated with 0.1% Triton X-100 (Sigma) for 10 min and incubated with 5% bovine serum albumin (ThermoFisher Scientific) for 1 h at RT. ICAM-1 monoclonal antibody (ThermoFisher Scientific) was incubated overnight at 4 °C at a concentration according to the manufacturer recommendations. After washing in PBS (ThermoFisher Scientific), samples were incubated with secondary antibody for 1 h at RT. Images were acquired with a Nikon confocal microscope and processed with Fiji software for morphological analyses. For live imaging within microfluidic chips, neutrophils were stained with Hoechst 33342 (Thermofisher Scientific) for 30 min at 37 °C immediately after blood component isolation.

2.10. Statistics

Statistical differences between experimental groups were quantified through Student's t-test (Prism Graph Pad), unless specified in the figure legend. Differences were considered significant for $p < 0.05$ (*), $p < 0.01$ (**), $p < 0.001$ (***) and $p < 0.0001$ (****). Results are presented as mean ± standard deviation (SD).

3. Results

3.1. Development of a perfusable vascularized breast cancer metastasis into bone-mimicking microenvironment

We firstly verified the possibility to obtain a mineralized hydrogel to

mimic a bone-mimicking microenvironment through the embedding of O-BMSCs (i.e. BMSCs pre-cultured with osteo differentiation medium for 14 days). To test their mineralization, cells were seeded in monolayer (Supplementary Fig. 1A) and subsequently embedded in fibrin hydrogel (Supplementary Fig. 1B) to better mimic the condition within the device. Both samples were fixed and stained with OsteoImage mineralization assay, showing the expression of hydroxyapatite secreted by O-BMSCs (Supplementary Figs. 1A and B), which is a hallmark of proper cell differentiation.

The design of the microfluidic device was inspired by previously validated configurations [20,27] to ensure the proper supply of nutrients to the cells and gas exchanges. Since the goal of this study is the generation of perfusable metastatic seeds surrounded by a bone-specific microenvironment, here we introduced three circular hydrogel regions flanked by two hydrogel channels containing perfusable microvascular networks (Fig. 1A). These microvascular networks are only connected through the central hydrogel regions and allow communication between the external media channels. This feature is meant to guarantee that anything (e.g. solutes, particles, cells) flowing through the microvessels from one medium channel to the other one crosses the metastasis circular regions.

The microfluidic chip was designed to fulfill a specific requirement, namely the confinement of the hydrogel matrices within the hydrogel channels and the circular regions while keeping them in direct contact. The confinement of the hydrogels was obtained through the use of lips of PDMS placed on the top of the microfluidic channels at the interface between two separate regions (e.g. circular hydrogel regions and hydrogel channels). To prove the communication between ECs embedded in both hydrogels and the formation of a continuum microvascular network, we seeded GFP-ECs in the two hydrogel channels and RFP-ECs in the central circular regions without adding CCs for these initial tests. After 4 days of culture, we observed the successful formation of a unique microvascular network connecting the two hydrogel regions of the device (Fig. 1C). We observed that at the interface of the two hydrogels, GFP/RFP ECs were able to interact, contributing to the creation of hybrid vessels where these two cell populations together formed the endothelial wall of the same microvessel (Fig. 1C).

To assess if the observed connection between ECs led to the formation of perfusable vessels, we injected 70 kDa TRITC Dextran (Fig. 1D, Supplementary Video 1) also in presence of CCs in the circular regions. Dextran injection demonstrated the complete connection of the two microvascular networks developed within the device and the perfusion of the whole BMtB microenvironment.

In particular, it was possible to observe how the solute starting from one media channel (below) flowed within the microvascular network crossing the metastasis region, perfused the network developed in the other hydrogel channel and finally reached the (upper) medium channel. Next, neutrophils were injected into these microvascular networks proving that circulating immune cells can actually reach the metastasis region where they can interact with CCs. Overall, these results confirmed that the design of the microfluidic device enabled the achievement of the original goal to perfuse circulating immune cells inside an already formed BMtB through functional microvascular networks.

3.2. CCs damage the microvascular network structure and permeability

Although we proved that microvascular networks remained perfusable in presence of CCs, we sought to determine if the BMtB microenvironment could induce changes to their architecture. To do this, we quantified the differences between microvascular networks developed into the circular hydrogel regions with and without CCs. Microvascular network patterns were identified using Fiji plugins (Fig. 2A). Our results showed that while the surface area occupied by the networks without and with CCs was similar (37.60 ± 2.50 vs. 33.68 ± 1.90 [%], $p = 0.254$) (Fig. 2B), the architecture of the network significantly changed (Fig. 2C, D, E). Indeed, comparing the number of independent network branches we observed lower values in samples without CCs (25.78 ± 3.73 vs. 43.00 ± 5.52, $p = 0.018$) (Fig. 2E), corresponding to a more interconnected structure of the network. This result was confirmed by the higher number of junctions detected in the absence of CCs (18.80 ± 4.51 vs. 5.70 ± 1.16, $p = 0.0257$) (Fig. 2C). Moreover, without CCs we also observed a higher network length (13.40 ± 0.82 vs. 10.49 ± 1.04 [mm], $p = 0.0426$) (Fig. 2D).

Finally, we quantified the permeability of microvascular networks (Fig. 2F and G), which is another feature of the vasculature that is known to be affected by the presence of CCs [28]. Our results validated *in vivo* observations showing that the permeability of the network was significantly higher when measured in presence of CCs ($2.60 \times 10^{-8} \pm 3.59 \times 10^{-8}$ vs. $0.53 \times 10^{-8} \pm 0.44 \times 10^{-8}$ [cm/s], $p = 0.05$) (Fig. 2F).

3.3. The metastatic-like microenvironment promotes neutrophil extravasation

Freshly isolated neutrophils were stained with Hoechst 33342 (blue) before the injection into microvascular networks so that it was possible to track them and quantify their migration within the devices after 24 h incubation (day 5 from microfluidic device seeding). Z-stacks of the circular regions (10× magnification, 10 μm z-step) were acquired in real-time using a confocal microscope and then processed with Fiji software to compare the extravasation of neutrophils with and without CCs (Fig. 3A).

The percentage of extravasated neutrophils over the total number of neutrophils was significantly higher in presence of CCs (27.90 ± 13.67 vs. 14.72 ± 12.42 [%], $p = 0.01$) (Fig. 3B). This confirms that specific microenvironments (i.e. BMtB and healthy bone tissue without CCs) can be generated in the microfluidic device to condition the behavior of circulating immune cells (i.e. neutrophils), hence mimicking the *in vivo* observed recruitment of neutrophils into tumors.

We also quantified the permeability of the vascular network in presence of neutrophils and/or cancer cells, showing that the permeability of the vasculature 24 h after neutrophil injection was similar comparing the metastatic (CCs + N) and the healthy bone-mimicking microenvironment (noCCs + N) ($2.04 \times 10^{-8} \pm 1.87 \times 10^{-8}$ vs. $1.77 \times 10^{-8} \pm 1.38 \times 10^{-8}$ [cm/s], $p = 0.8555$) (Fig. 3D). This suggests that in presence of neutrophils CC did not induce an increase in vascular network permeability.

On the other hand, the presence of neutrophils significantly increased the permeability of the vasculature in presence of CCs, which ranged from $0.37 \times 10^{-8} \pm 0.49 \times 10^{-8}$ [cm/s] with only CCs to $2.04 \times 10^{-8} \pm 1.87 \times 10^{-8}$ [cm/s] with CCs + N ($p = 0.0045$). Surprisingly, the permeability of the endothelium exposed to neutrophils alone was even higher than that measured with CCs alone ($1.77 \times 10^{-8} \pm 1.38 \times 10^{-8}$ [cm/s] (noCCs + N) compared to $0.37 \times 10^{-8} \pm 0.49 \times 10^{-8}$ [cm/s] (CCs) ($p = 0.0244$) (Fig. 3D).

Since the higher extravasation of neutrophils could also be influenced by the higher expression of vascular adhesion molecules such as ICAM-1 [29], we then performed ICAM-1 immunofluorescence analysis and quantified EC-ICAM-1 colocalization area (%) over the total EC area. CCs also express ICAM-1, thus CC-ICAM-1 signal was subtracted from the EC-ICAM-1 signal. The resulting ICAM-1 expressed by ECs did not show any significant difference with or without CCs (30.40 ± 10.14 (CCs); 26.74 ± 9.53 (CCs + N); 25.62 ± 4.26 (noCCs + N) [%]) (Fig. 3C). This result suggests that the higher extravasation of neutrophils in presence of CCs in our system is not mediated by changes in ICAM-1 expression. Rather, it might be possible that CCs promote neutrophil extravasation through secreted factors, although further analyses would be required to verify which specific molecules secreted by CCs drive the recruitment of neutrophils.

Overall, our data confirm that short-term (24 h) interactions between ECs and neutrophils are sufficient to modify the barrier permeability of microvascular networks and that the presence of CCs increases neutrophil extravasation.

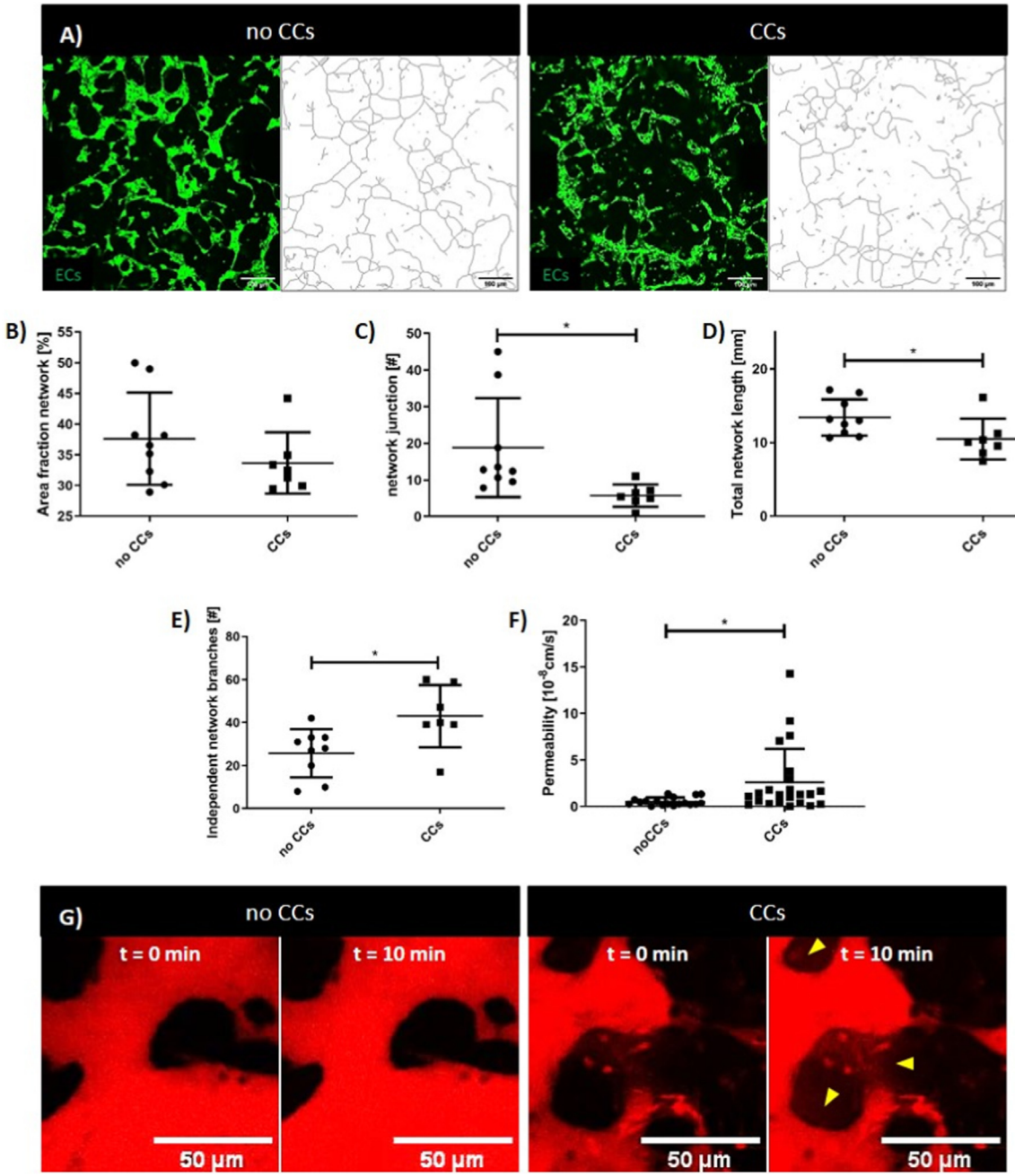

Fig. 2. CCs affect microvascular network architecture and permeability. Representative confocal images of microvascular networks (green) developed within the circular regions after 4 days of culture without and with CCs and schematic of the networks obtained through Analyze Skeleton plugin (A). Data obtained by the analysis of the network (n = 16): percentage of the area occupied by the network (B), number of junctions between the branches of the network (C), total length of the network (D), number of independent network structures developed within the analyzed area (E). Data obtained by the analysis of the permeability showing higher leakage in presence of CCs. Data obtained by three different experiments, at least n = 18 ROIs for each condition (F). Representative confocal images showing 70 kDa Dextran (red) perfusion within networks without and with CCs comparing the initial (t = 0 min) and final (t = 10 min) time points (G). (For interpretation of the references to colour in this figure legend, the reader is referred to the Web version of this article.)

3.4. Neutrophils affect CC viability in bone-mimicking metastatic microenvironment

To characterize the interaction between neutrophils and CCs we initially performed simplified co-culture assays. The first model was a 2D co-culture of freshly isolated neutrophils from buffy coats of healthy human donors put in suspension on top of previously seeded CC monolayers. Surprisingly after 24 h of CC-neutrophil co-culture, CCs were almost entirely detached (Supplementary Fig. 2A). This result was consistently obtained with three different blood donors and quantified in terms of Area Fraction (the percentage of the area of the image covered by the cells). The result showed that the CC monolayer was significantly reduced by the co-culture with neutrophils (0.90 ± 0.20 vs. 16.91 ± 3.15 [%], $p < 0.0001$) (Supplementary Fig. 2B).

To exclude possible biases due to the 2D co-culture, we then seeded CCs in 3D hydrogel droplets and measured CC viability using Draq7 staining (Supplementary Fig. 2C) with or without neutrophils in the culture medium surrounding the droplets. The results showed a significantly higher mortality when CCs were in presence of neutrophils (1.00 ± 1.25 vs. 25.54 ± 26.84 [n/µm^2], $p < 0.0001$) (Supplementary Fig. 2D).

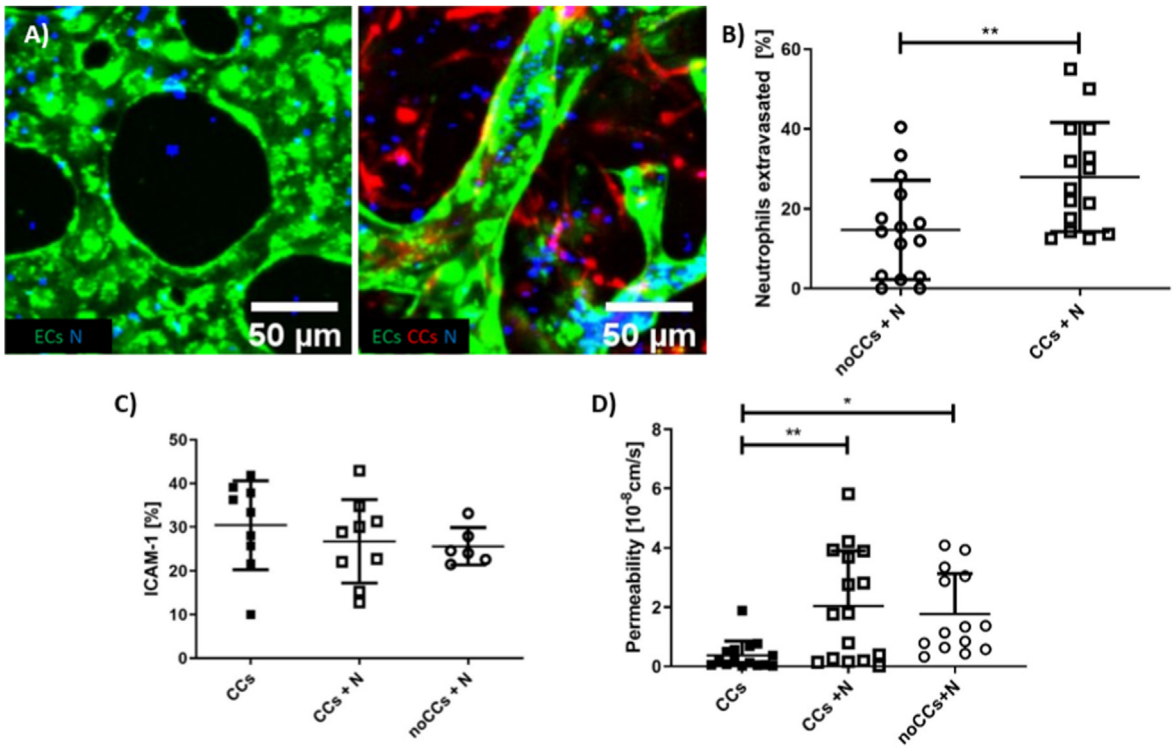

Fig. 3. Neutrophil migration within the device and interaction with ECs. Representative confocal images (200 μm × 200 μm) showing neutrophils (N, blue) within microvascular networks (green). More neutrophils are located in the extravascular space when CCs (red) are present, 10× magnification (A). Data reporting the quantification of the % neutrophil extravasated (n = 15 for each condition, neutrophils isolated from one blood donor) (B). Quantification of the % colocalized area (EC-ICAM-1) in three different conditions: BMtB with CCs, BMtB with CCs and neutrophil perfusion (CCs + N), healthy bone-mimicking microenvironment with neutrophils (noCCs + N) (at least n = 6 for each condition, neutrophils isolated from two blood donors) (C). Quantification of microvascular network permeability in the same conditions reported in C (at least n = 14 for each condition, neutrophils isolated from two blood donors) (D). (For interpretation of the references to colour in this figure legend, the reader is referred to the Web version of this article.)

This quantification demonstrated the cytotoxic role of neutrophils in our *in vitro* setup, confirming previously published data [7] which pointed at the potential role of neutrophil-secreted ROS in inducing cell death [30]. We then verified the production of ROS in our system, finding a slight increase in the co-culture condition (16.74 ± 0.58 in CCs + N vs. 15.68 ± 0.50 in CCs, p = 0.1904), although not significant (Supplementary Fig. 2E).

We have also performed a preliminary experiment to characterize neutrophil changes following their interaction with breast CCs. Flow cytometry results suggest that neutrophils shift towards the N1 anti-tumoral phenotype after co-culture with CCs (Supplementary Fig. 3). This preliminary data appears to be in accordance with the increased CC death in presence of neutrophils observed in Fig. 3 and in Supplementary Fig. 2. We observed that neutrophils co-cultured with CCs increased the expression of two pro-apoptotic factors related to N1 polarization, namely TNF-α (CD120α and β) and FAS (CD95) receptors. We also reported a slightly increased expression of a marker of monocyte activation (CD15) and of the programmed cell death ligand 1 (CD274).

We then analyzed if the same anti-tumor behavior of neutrophils was also present in the BMtB model, quantifying CC death 24 h after the injection of neutrophils into microvascular networks (Fig. 4A and B). Through image analysis (see methods above), we were able to compare CC death in the complete BMtB microenvironment with and without neutrophils (CCs + N and CCs, respectively). The bone-mimicking microenvironment without CCs (noCCs + N) was added as control. The overall cellular death was not statistically different among all tested conditions (135.80 ± 86.09 (CCs); 178.80 ± 107.80 (CCs + N); 136.60 ± 111.80 (noCCs + N)) (Fig. 4C), proving that there was not a general cytotoxic effect due to the introduction of neutrophils. To specifically analyze CC death, we then looked at the colocalization of Draq7 signal with CCs (Fig. 4D). Although the percentage of dying CCs was low, it significantly increased with the addition of neutrophils (1.83 ± 1.76 vs. $1.48 \times 10^{-5} \pm 2.00 \times 10^{-5}$ [%], p = 0.0013). This result confirmed the cytotoxic effect of neutrophils on CCs, in agreement with our preliminary experiments and with the literature [7,31].

To further confirm the obtained results, we also analyzed CC viability through flow cytometry following cell isolation from the device. We considered as dead CCs those cells positive for both APC-A (Draq7 signal) and PE-A (CC RFP signal). The number of double positive cells increased with the addition of neutrophils as compared to CCs alone (11.90% vs. 7.08%) (Fig. 4E), hence confirming the results obtained on-chip with confocal imaging. Furthermore, these results demonstrate the possibility to successfully collect and analyze single cell populations from a complex 3D microenvironment within a microfluidic chip, fostering the application of quantitative techniques (e.g. flow cytometry) to microscale, bio-fabricated models.

We also set an additional test to verify that the different mortality rate observed in simplified 2D/3D cultures compared to the complex bio-fabricated 3D model was not only due to the different setup of the experiments. More into detail, we compared 3D hydrogel droplets of CCs alone and CCs co-cultured with cells of the bone-mimicking microenvironment. The presence of the bone-mimicking microenvironment significantly reduced the neutrophil killing effect on CCs (25.57 ± 5.263 vs. 67.16 ± 7.617 [%], p < 0.0001) (Supplementary Fig. 4), proving that stromal cells play a protective role for CCs [32]. This result also confirms the importance of reproducing the cellular heterogeneity of the bone metastatic region to properly mimic the cell-cell interactions occurring during cancer progression.

Finally, we tried a preliminary test to pre-polarize neutrophils with TGF-β1 (10 ng/ml) or with CC conditioned media. We quantified

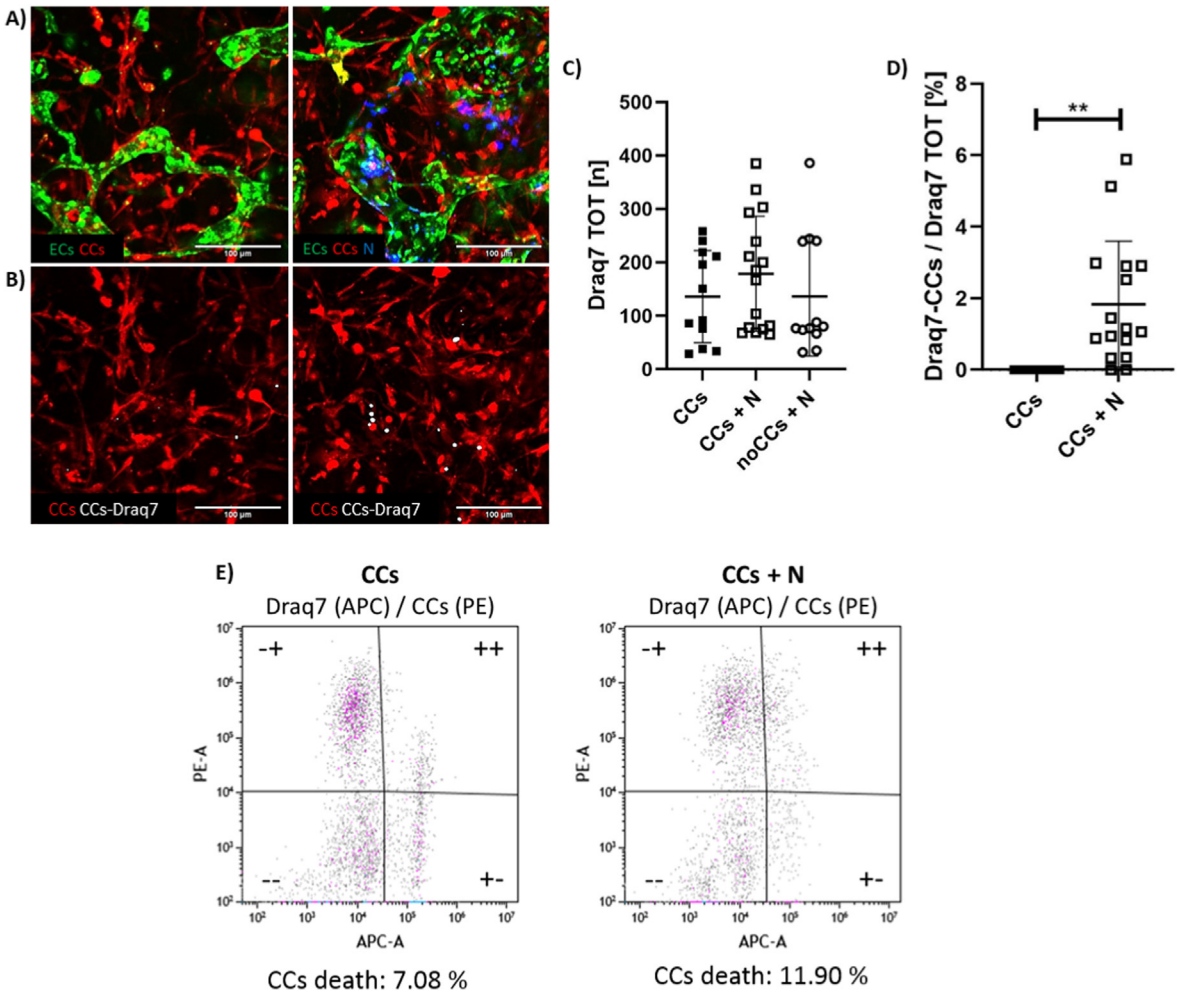

Fig. 4. CC death in presence of neutrophils. Representative confocal images (300 μm × 300 μm) showing microvascular networks (green), CCs (red) and neutrophils (N, blue) 24 h after neutrophil injection. These images show two experimental conditions: complete BMtB microenvironment with and without neutrophils, 10× magnification (A). Representative confocal images showing CCs (red) and the colocalization of CCs and Draq7 signal (white), 24 h after neutrophil injection. The CC (red) signal corresponds to images reported in A. 10× magnification (B). Quantification of the total death of all the cells embedded in the hydrogel of each microenvironment (neutrophils excluded), expressed as the number of Draq7 spots, which correspond to nuclei of dead cells (at least n = 12 for each condition, neutrophils isolated from two blood donors) (C). Quantification of the percentage of Draq7 signal colocalized with CCs over the total amount of Draq7 (D). Graph plotting CC granularity with and without neutrophils, PE-A corresponding to CC RFP signal (ordinate) vs. APC-A corresponding to Draq7 FarRed signal (abscissa) (E). (For interpretation of the references to colour in this figure legend, the reader is referred to the Web version of this article.)

neutrophil polarization through immunofluorescence staining of N1 markers (i.e. ICAM-1 and TNFα) and N2 markers (i.e. MMP9 and VEGF) considering two different time points (2 and 24 h). Live and dead assay showed that almost 100% neutrophils were alive at both time points in each condition. We did not quantify any significant difference in the expression of N1 or N2 markers compared to control conditions (Supplementary Fig. 5). Overall, this preliminary observation suggests that direct contact with CCs might be necessary to trigger neutrophil polarization or that longer incubation with the metastatic microenvironment is required to change the neutrophil phenotype.

4. Discussion

Based on the experience of our lab in developing complex 3D *in vitro* models featuring specific microenvironments [20,33,34], in this work we designed a microfluidic model of human vascularized BMtB that allowed us to quantitatively characterize the interaction between circulating neutrophils and breast CCs. To define the model, especially for what concerns the choice of the cellular components, we were inspired by results previously obtained by our lab. In particular, we previously demonstrated that breast CCs co-cultured with bone-resident cells (i.e. osteoblasts, osteoclasts, macrophages, ECs) acquire a specific phenotype. Indeed, breast CCs overexpress bone-specific markers (e.g. TRAP) in a process called osteo-mimicry and differentially respond to chemotherapies compared to monoculture conditions [24]. Moreover, we have already demonstrated that a bone microenvironment can partially promote the organ-specific differentiation of ECs towards a bone-specific phenotype [35]. Previous studies mainly analyzed neutrophil-CC interactions through *in vivo* models or traditional 2D *in vitro* systems. *In vivo* models capture the complexity of living organisms, although species-specific differences characterize the immune system, hence potentially affecting the translation of the obtained results to a human setting. At the same time, simplified 2D *in vitro* systems using human cells do not generally consider the role of the endothelium and the tridimensionality of the biological microenvironment that affect both the growth of metastatic tumors and the circulation/homing of immune cells. To fill this gap, here we focused on the development of a microfluidic device that allows neutrophil perfusion through an interconnected microvascular network that crosses an already established breast cancer metastasis region within the bone-mimicking microenvironment. Although similar models involving the culture of vascularized tumor spheroids in a microfluidic chip have already been published [36,37],

our model also includes the presence of a bone-mimicking microenvironment, thus allowing the investigation of bone metastases within a physiological-like model.

Particular attention was dedicated to adjust the design of the microfluidic device, achieving the confinement of the hydrogels while maintaining their direct contact. We demonstrated the perfusability and the interconnection of the microvascular networks across the different compartments with the injection of 70 kDa TRITC Dextran and prestained neutrophils. Importantly, we compared the vasculogenesis in healthy and tumor microenvironments, showing that the vascular network in presence of CCs was more chaotic, less interconnected and leakier, in accordance with what has been already observed *in vivo* [28].

The plasticity showed by some components of the immune system in response to the tumor microenvironment has become a relevant aspect for understanding tumor progression and represents a promising therapeutic target. In this work, we specifically focused on TANs, which have been recently classified in N1 anti- and N2 pro-tumor phenotypes [38] following the previous classification of macrophage polarization. Within the microfluidic model, we quantified an anti-tumor behavior of neutrophils in the BMtB microenvironment, in agreement with previous studies [7,31]. We also observed that the presence of CCs increased neutrophil expression of N1 polarization markers (e.g. TNF Receptor I and II and FAS receptors, data not shown) which are an indication of anti-tumor phenotype [30]. These observations are in agreement with previous reports showing that neutrophils can induce CC lysis and apoptosis through a plethora of cytotoxic mediators, such as ROS [30], proteases, membrane-perforating agents and soluble mediators (e.g. TNF-α and IL-1β) [7]. The cytotoxicity of neutrophils was previously demonstrated on adherent cell lines of diverse tumor types without affecting the viability of other cell populations such as human fibroblasts [39]. In particular, *in vitro* direct co-culture models of neutrophils and CCs were reported to cause neutrophil singlet oxygen ($^1O_2$) production, which impairs CC proliferation [7]. Further, direct co-cultures also proved that neutrophils were able to selectively kill CCs through the release of active neutrophil elastase, only in case of human cells [31].

Neutrophil behavior and polarization are driven by a plethora of factors secreted by the tumor microenvironment. The stimuli sensed by neutrophils range according to the stage of tumor progression [40] and are mediated by other cellular elements. In particular, the blood vessel endothelium plays a fundamental role in the migration of neutrophils towards the tumor [11]. This aspect is particularly relevant in specific contexts, such as the bone microenvironment, which is characterized by high vascularization implying a continuous interaction with circulating immune cells [41]. Within our model, we quantified a higher extravasation rate of neutrophils in presence of CCs, confirming the accumulation of this immune cell population in the metastatic niche already reported in the literature [11]. The higher extravasation rate of neutrophils and their cytotoxic effect are also associated with a change in vascular permeability. However, when neutrophils were present we found no difference in permeability with and without CCs, indicating that increased neutrophil extravasation in presence of CCs is not dependent on increased vessel permeability and thus suggesting that neutrophil migration might be promoted by CC secreted factors [11]. Interestingly, neutrophils themselves increased the vascular permeability irrespectively from the presence of CCs, in agreement with previous studies that correlated the presence of neutrophils with leakier vessels [42]. Neutrophil adhesion on the endothelium was previously associated with the increased expression of endothelial surface molecules (e.g. ICAM-1) [29]. Our data did not show any significant increase in ICAM-1 expression in the BMtB microenvironment, suggesting either that other surface markers might be involved or that the different extravasation rate of neutrophils was not associated with a different adhesion on the endothelium.

CC viability within the device was quantified through real time high-resolution imaging. In addition, single cell populations were extracted from the metastatic regions and analyzed through flow cytometry. Importantly, both methodologies showed increased CC mortality when the BMtB microenvironment was perfused with neutrophils. Although the overall CC mortality rate was low, this result is in accordance with the one obtained in our 2D preliminary tests. Nevertheless, this comparison suggests that a simplified model might improperly overestimate an event such as neutrophil-dependent CC death. Indeed, within the microfluidic model here developed, the interaction between CCs and neutrophils was significantly different, especially considering the reduced number of contacts that neutrophils could have with CCs compared to 2D assays. The microenvironment biofabricated in the microfluidic device better mimics the pathological condition of a bone metastasis where a limited number of neutrophils flow within microvascular networks, arrest on the endothelial lumen, experience the chemo-attractive signals produced by the microenvironment, extravasate, migrate and finally reach the CC microenvironment [29]. Importantly, the possibility to extract cells from the metastatic seeds inside the microfluidic device could be further exploited. This feature might allow to better clarify other key aspects of the bone metastatic dissemination, such as the role of ECs in neutrophil extravasation, the different polarization of neutrophils and the biological mechanisms underlying CC death.

We would like to highlight that we did not add any external factors that artificially precondition both neutrophils and the microenvironment, as was instead reported in other works [21,43]. This choice prevents the overlapping of multiple signals, which might either modify the cell behavior or produce a side effect on the microenvironment (e.g. the microvasculature). At the same time, a limitation of this model is its short lifespan which reduces the time window to monitor the interactions between neutrophils, CCs and the microenvironment, thus impairing the possibility to observe or even control the polarization of neutrophils which *in vivo* occurs over longer time intervals [40]. A potential approach to overcome this limitation could be the setup of a dynamic perfusion system, which should contribute to the maintenance of the network integrity for a longer time. Another possible solution is inspired by a recent study in which a cocktail of specific factors to drive the polarization of human neutrophils towards either N1 or N2 phenotypes has been developed [44]. Pre-treating neutrophils with these cocktails before the injection in the microfluidic device could allow the observation of the different behavior of polarized neutrophils in the microenvironment as well as to test some potential treatments to boost the N1 phenotype or reverse the N2.

5. Conclusions

In conclusion, in this work we designed and developed an effective 3D microfluidic model that for the first time reproduced a perfusable vascularized breast cancer metastasis within the bone-mimicking microenvironment, enabling the analysis of immune/EC/CC interactions. This model allowed us to observe the influence of CCs on vessel formation, the effect of the metastatic bone-mimicking microenvironment on neutrophil extravasation and the neutrophil-mediated CC death. We believe that this model could help to identify key aspects of neutrophil behavior in bone metastases, possibly leading to the development of innovative anti-metastatic treatments combining traditional chemotherapies with novel immunotherapies.

Funding

This research was funded by the Swiss National Science Foundation through the grant number SNF 310030_179167.

Author contributions

Conceptualization, M.C., C.A., S.Be. and M.M.; methodology, M.C., G.T., A.L., S. Bo. and S.Be; data curation, M.C.; writing—original draft

preparation, M.C.; writing—review and editing, C.A., S.Be. and M.M.; supervision, S.Be. an M.M.; funding acquisition, M.M. All authors have read and agreed to the published version of the manuscript.

Declaration of competing interest

The authors declare that they have no known competing financial interests or personal relationships that could have appeared to influence the work reported in this paper.

Data availability

Data will be made available on request.

Appendix A. Supplementary data

Supplementary data to this article can be found online at https://doi.org/10.1016/j.mtbio.2022.100460.

References

[1] K. Ganesh, J. Massagué, Targeting metastatic cancer, Nat. Med. 27 (2021) 34–44.
[2] G.R. Mundy, Metastasis to bone: causes, consequences and therapeutic opportunities, Nat. Rev. Cancer 2 (2002) 584–593.
[3] L.J. Suva, R.J. Griffin, I. Makhoul, Mechanisms of bone metastases of breast cancer, Endocr. Relat. Cancer 16 (2009) 703–713.
[4] L. Xiang, D.M. Gilkes, The contribution of the immune system in bone metastasis pathogenesis, Int. J. Mol. Sci. 20 (2019).
[5] O.S. Blomberg, L. Spagnuolo, K.E. De Visser, Immune regulation of metastasis: mechanistic insights and therapeutic opportunities, DMM Dis. Model. Mech. 11 (2018).
[6] L.M.E. Janssen, E.E. Ramsay, C.D. Logsdon, W.W. Overwijk, The immune system in cancer metastasis: friend or foe? J. Immunother. Cancer 5 (2017) 1–14.
[7] H. Piccard, R.J. Muschel, G. Opdenakker, On the dual roles and polarized phenotypes of neutrophils in tumor development and progression, Crit. Rev. Oncol. Hematol. 82 (2012) 296–309.
[8] A. Sica, P. Allavena, A. Mantovani, Cancer related inflammation: the macrophage connection, Cancer Lett. 267 (2008) 204–215.
[9] G. Solinas, G. Germano, A. Mantovani, P. Allavena, Tumor-associated macrophages (TAM) as major players of the cancer-related inflammation, J. Leukoc. Biol. 86 (2009) 1065–1073.
[10] Z.G. Fridlender, S.M. Albelda, Tumor-associated neutrophils: friend or foe? Carcinogenesis 33 (2012) 949–955.
[11] S. Jaillon, et al., Neutrophil diversity and plasticity in tumour progression and therapy, Nat. Rev. Cancer 20 (2020) 485–503.
[12] Z.G. Fridlender, et al., Polarization of tumor-associated neutrophil phenotype by TGF-beta: 'N1' versus 'N2' TAN, Cancer Cell 16 (2009) 183–194.
[13] A.D. Gregory, A.M.G. Houghton, Tumor-associated neutrophils: new targets for cancer therapy, Cancer Res. 71 (2011) 2411–2416.
[14] Z. Granot, et al., Tumor entrained neutrophils inhibit seeding in the premetastatic lung, Cancer Cell 20 (2011) 300–314.
[15] M. Gershkovitz, et al., Microenvironmental cues determine tumor cell susceptibility to neutrophil cytotoxicity, Cancer Res. 78 (2018) 5050–5059.
[16] Dirk J. van der Windt, Sud Vikas, Hongji Zhang, Patrick R. Varley, Julie Goswami1, Hamza O. Yazdani, Samer Tohme, Patricia Loughran, M. Robert, Doherty O', I. Minervini Marta, Huang Hai, L. Simmons Richard, Tsung Allan, J. Dirk, der van, A. T. Inflammation and development of hepatocellular, Hepatology 68 (4) (2019) 1347–1360, https://doi.org/10.1002/hep.29914, 2018 Oct.
[17] Z. Zhou, et al., Tumor-associated neutrophils and macrophages interaction contributes to intrahepatic cholangiocarcinoma progression by activating STAT3, J. Immunother. cancer 9 (2021).
[18] L.A. Mittmann, et al., Uncoupled biological and chronological aging of neutrophils in cancer promotes tumor progression, J. Immunother. cancer 9 (2021).
[19] M. Chen, et al., Neutrophils as emerging immunotherapeutic targets: indirect treatment of tumors by regulating the tumor immune environment based on a sialic acid derivative-modified nanocomplex platform, Int. J. Pharm. 121684 (2022), https://doi.org/10.1016/j.ijpharm.2022.121684.
[20] M. Crippa, et al., A microphysiological early metastatic niche on a chip reveals how heterotypic cell interactions and inhibition of integrin subunit β3impact breast cancer cell extravasation, Lab Chip 21 (2021) 1061–1072.
[21] M.B. Chen, et al., Inflamed neutrophils sequestered at entrapped tumor cells via chemotactic confinement promote tumor cell extravasation, Proc. Natl. Acad. Sci. U.S.A. 115 (2018) 7022–7027.
[22] S. Han, et al., A versatile assay for monitoring in vivo-like transendothelial migration of neutrophils, Lab Chip 12 (2012) 3861–3865.
[23] S. Bersini, et al., A microfluidic 3D in vitro model for specificity of breast cancer metastasis to bone, Biomaterials 35 (2014) 2454–2461.
[24] M.V. Colombo, et al., Engineering the early bone metastatic niche through human vascularized immuno bone minitissues, Biofabrication 13 (2021).
[25] M. Bongio, S. Lopa, M. Gilardi, S. Bersini, M. Moretti, A 3D vascularized bone remodeling model combining osteoblasts and osteoclasts in a CaP nanoparticle-enriched matrix, Nanomedicine (2016), https://doi.org/10.2217/nnm-2015-0021.
[26] G.S. Offeddu, et al., Application of transmural flow across in vitro microvasculature enables direct sampling of interstitial therapeutic molecule distribution, Small 15 (2019) 1–10.
[27] J.S. Jeon, et al., Erratum: human 3D vascularized organotypic microfluidic assays to study breast cancer cell extravasation (Proc. Natl. Acad. Sci. U.S.A. (2015) 112:1 DOI: 10.1073/pnas.1501426112 (214-219)), Proc. Natl. Acad. Sci. U. S. A. 112 (2015) E818.
[28] G. Bergers, L.E. Benjamin, Tumorigenesis and the angiogenic switch, Nat. Rev. Cancer 3 (2003) 401–410.
[29] E. Di Carlo, et al., The intriguing role of polymorphonuclear neutrophils in antitumor reactions, Blood 97 (2001) 339–345.
[30] E. Pylaeva, S. Lang, J. Jablonska, The essential role of type I interferons in differentiation and activation of tumor-associated neutrophils, Front. Immunol. 7 (2016) 629.
[31] C. Cui, et al., Neutrophil elastase selectively kills cancer cells and attenuates tumorigenesis, Cell 184 (2021) 3163–3177, e21.
[32] K.M. Bussard, L. Mutkus, K. Stumpf, C. Gomez-Manzano, F.C. Marini, Tumor-associated stromal cells as key contributors to the tumor microenvironment, Breast Cancer Res. 18 (2016) 1–11.
[33] S. Bersini, et al., Human in vitro 3D co-culture model to engineer vascularized bone-mimicking tissues combining computational tools and statistical experimental approach, Biomaterials 76 (2016) 157–172.
[34] S. Bersini, et al., Engineered miniaturized models of musculoskeletal diseases, Drug Discov. Today (2016), https://doi.org/10.1016/j.drudis.2016.04.015.
[35] S. Bersini, et al., Engineering an environment for the study of fibrosis: a 3D human muscle model with endothelium specificity and endomysium, Cell Rep. 25 (2018) 3858–3868, e4.
[36] K. Haase, G.S. Offeddu, M.R. Gillrie, R.D. Kamm, Endothelial regulation of drug transport in a 3D vascularized tumor model, Adv. Funct. Mater. 30 (2020).
[37] Y. Nashimoto, et al., Vascularized cancer on a chip: the effect of perfusion on growth and drug delivery of tumor spheroid, Biomaterials 229 (2020).
[38] Z.G. Fridlender, et al., Polarization of tumor-associated neutrophil phenotype by TGF-β: 'N1' versus 'N2' TAN, Cancer Cell 16 (2009) 183–194.
[39] T.L. Gerrard, D.J. Cohen, A.M. Kaplan, Human neutrophil-mediated cytotoxicity to tumor cells, J. Natl. Cancer Inst. 66 (1981) 483–488.
[40] M.E. Shaul, et al., Tumor-associated neutrophils display a distinct N1 profile following TGFβ modulation: a transcriptomics analysis of pro- vs. antitumor TANs, OncoImmunology 5 (2016) 1–14.
[41] M. Esposito, T. Guise, Y. Kang, The biology of bone metastasis, Cold Spring Harb. Perspect. Med. 8 (2018).
[42] V.A. Naumenko, et al., Extravasating neutrophils open vascular barrier and improve liposomes delivery to tumors, ACS Nano 13 (2019) 12599–12612.
[43] V. Surendran, D. Rutledge, R. Colmon, A. Chandrasekaran, A novel tumor-immune microenvironment (TIME)-on-Chip mimics three dimensional neutrophil-tumor dynamics and neutrophil extracellular traps (NETs)-mediated collective tumor invasion, Biofabrication 13 (2021).
[44] M. Ohms, S. Möller, T. Laskay, An attempt to polarize human neutrophils toward N1 and N2 phenotypes in vitro, Front. Immunol. 11 (2020) 1–12.